Biosensors and Bioelectronics 64 (2015) 477–484

Contents lists available at ScienceDirect

Biosensors and Bioelectronics

journal homepage: www.elsevier.com/locate/bios

Highly-ordered perpendicularly immobilized FWCNTs on the thionine monolayer-modified electrode for hydrogen peroxide and glucose sensors

Min Ma, Zhiying Miao, Di Zhang, Xin Du, Yanyan Zhang, Cong Zhang, Jiahui Lin, Qiang Chen *

The Key Laboratory of Bioactive Materials, Ministry of Education, College of Life Science, Nankai University, Weijin Road No. 94, Tianjin 300071, PR China

ARTICLE INFO

Article history:
Received 26 July 2014
Received in revised form
6 September 2014
Accepted 22 September 2014
Available online 28 September 2014

Keywords:
Perpendicularly aligned few-walled carbon nanotubes
11-amino-n-undecanethiol
Thionine
Pt nanoparticles
Non-enzymatic hydrogen peroxide sensors
Glucose biosensor

ABSTRACT

In this paper, we innovatively immobilized few-walled carbon nanotubes (FWCNTs) perpendicularly on Au surface through conductive thionine instead of aminoalkanethiols so as to improve electrochemical properties. Because FWCNTs own smaller aggregates, stronger chemical corrosion resistant, and higher conductivity than single-walled carbon nanotubes (SWCNTs), and thionine is a good electron transfer mediator can provide amino and sulfhydryl groups playing the same function as insulating aminoalkanethiols. The strategy for obtaining perpendicularly aligned FWCNTs (p-FWCNTs) is electrostatically assembled thionine and 11-amino-n-undecanethiol (AUT) on Au surface via Au-S bond to provide amino groups for covalently combining terminus-carboxylated FWCNTs, we confirmed and compared the results by AFM, Raman spectroscopy and electrochemical methods. In order to prove the constructed basement has excellent electrochemical properties can provide a good platform for sensors fabrication, we developed a novel non-enzymatic hydrogen peroxide (H_2O_2) sensor by electrodepositing Pt nanoparticles (PtNPs) on p-FWCNTs/Thionine/Au electrode surface, and verified the result by TEM, EDX and electrochemical techniques. Furthermore, polyallylamine (PAA) and poly(vinyl sulfate) (PVS) permselective layer, poly(diallyldimethylammonium) (PDDA) and glucose oxidase (GO_x) multilayer films were layer-by-layer self-assembled on p-FWCNTs/Thionine/Au surface to fabricate a glucose biosensor. Either the non-enzymatic H_2O_2 sensor or the enzyme-based glucose biosensor showed good sensitivity, selectivity, reproducibility and stability, both them had been applied for biological sample analysis with satisfactory results. The results show that the p-FWCNTs/Thionine/Au electrode can work as an ideal platform for the development of highly sensitive sensors, coupled with p-FWCNTs are rich in functional groups could be used for fabricating diverse sensors.

1. Introduction

Carbon nanotubes (CNTs) have received a great deal of interest for their superior electrical (Baughman et al., 2002), mechanical (Nayak et al., 2012) and thermal (Heer et al., 1995) properties originating from one-dimensional all-carbon structure (Ouyang et al., 2002). CNTs can be divided into three types: single-walled carbon nanotubes (SWCNTs), few-walled carbon nanotubes (FWCNTs), and multi-walled carbon nanotubes (MWCNTs). SWCNTs are intensive research subject in designing sensors for their interesting structural and electrical properties (McEuen et al., 2002). FWCNTs show ideal one-dimensional structure as SWCNTs, while form aggregates less effectively than SWCNTs (Qi et al., 2006; Qian et al., 2007). Furthermore, FWCNTs can maintain the structural integrity of the inner layers even if the outermost layer is functionalized, because of their high stability against heat and chemical treatments (Qian et al., 2006). Moreover, conductivity and field emission performance of FWCNTs is stronger than SWCNTs.

Compared with tangled CNTs, vertically aligned CNTs have better mechanical stability, larger surface-to-volume ratio (Yang et al., 2008) and faster heterogeneous electron transfer (Chou et al., 2005). Therefore, perpendicularly ordered CNTs may be useful for improving the performance of nanotube-based electrochemical sensors. Vertically aligned CNTs can be obtained by chemical vapor deposition (Huang et al., 2007; Yan et al., 2007) or chemical assembly (Diao and Liu, 2010). The chemical vapor

* Corresponding author. Fax: +86 22 23506122.
E-mail address: qiangchen@nankai.edu.cn (Q. Chen).

http://dx.doi.org/10.1016/j.bios.2014.09.057
0956-5663/

deposition method requires metal catalysts, which is detrimental to the performance of sensors and less tolerant of CNTs functionalization. Recently, wet chemical approaches have been developed to immobilize SWCNTs onto solid surfaces (Peng et al., 2005; Gooding et al., 2003; Patolsky et al., 2004; Sheeney-Haj-Ichia et al., 2005). The route of chemical assembly involves end-functionalization of shortened SWCNTs, which are then immobilized onto aminoalkanethiols modified substrates via covalent or electrostatic interactions. For example, Liu et al. covalently assembled insulating monolayer of 11-amino-n-undecanethiol (AUT) on the Au substrate via Au-S bond, then fixed one end of pre-shortened and terminus-carboxylated SWCNTs on solid surfaces by amide bonds (Peng et al., 2005). However, the electron transport mechanism across insulating AUT is unclear. Therefore, we choose here thionine instead of AUT because thionine is a good electron transfer mediator can facilitate electron transfer between substrate and CNTs. In this study, we innovatively use thionine for developing a perpendicularly aligned FWCNTs (p-FWCNTs) layer on the surface of Au substrate by the electric field-assisted wet chemical approaches for the first time to the best of our knowledge.

Hydrogen peroxide (H_2O_2) is not only a commonly used oxidant in industrial processes, but also an important by-product of a large number of oxidase enzymes (Mattos et al., 2003). Platinum nanoparticles (PtNPs) is widely used in electrochemical detection of H_2O_2 for their high catalytic activities (Janyasupab et al., 2013; Chen et al., 2013). So we electrodeposited PtNPs on the p-FWCNTs/Thionine/Au electrode surface to fabricate a novel non-enzymatic H_2O_2 sensor. Since the measurement of glucose is important for the diagnosis and management of diabetes mellitus, and glucose oxidase (GO_x) is an ideal enzyme widespreadly used in biosensors for the catalytic ability to glucose (Liu et al., 2007). In earlier work, we successfully constructed satisfactory biosensors through layer-by-layer self-assembly technique involving an alternate adsorption of anionic and cationic polyelectrolytes including polyallylamine (PAA), poly(vinyl sulfate) (PVS) and poly(diallyldimethylammonium) (PDDA) based on the electrostatic interaction (Qin et al., 2009; Wu et al., 2009), So we also developed a $(PDDA/GO_x)_8/(PAA/PVS)_3$/p-FWCNTs/Thionine/Au glucose biosensor by the same technique for comparison. In this work, we studied both the non-enzymatic H_2O_2 sensor and enzyme-based glucose biosensor to prove the basement p-FWCNTs/Thionine/Au we have constructed owning excellent electrochemical properties could provide a good platform for fabricating diverse sensors.

2. Experimental

2.1. Reagents

Few-walled carbon nanotubes (FWCNTs) (< 6 lays) were purchased from Institute of Organic Chemistry, Chinese Academy of Sciences (Chengdu, China). Glucose oxidase from Aspergillus niger (GOD, EC 1.1.3.4), poly(diallyldimethylammonium chloride) (PDDA, MW: 40,000–50,000), poly(allylamine) (PAA, MW:10,000), poly (vinyl sulfate, potassium salt) (PVS, MW:170,000), Potassium Hexachloroplatinate (K_2PtCl_6), dicyclohexylcarbodiimide (DCC), thionine, uric acid, ascorbic acid, dopamine and acetaminophen were purchased from Sigma Aldrich Co. (USA). 11-amino-n-undecanethiol (AUT) was obtained from Dojindo (Japan). Hydrogen peroxide (H_2O_2, 30%) and glucose were purchased from Tianjin Eastern Chemical Reagent Co. (China). All other reagents were of analytical reagent grade and used as received without any further purification, and doubly distilled water was used throughout.

Freshly prepared 0.1 M phosphate buffer solution (PBS, pH 7.0) consisting of Na_2HPO_4 and NaH_2PO_4, 5 mM $[Fe(CN)_6]^{3-}$ solution containing 0.1 M KCl as the supporting electrolyte. All experiments were performed at room temperature, approximately 25 °C.

2.2. Apparatus and measurements

Electrochemical measurements were conducted with a potentiostat-galvanostat (Model 283 with a software M270, EG&G, PARC). A three-electrode system was employed with the modified Au electrode as the working electrode, a Pt wire as the auxiliary electrode and Ag/AgCl (saturated KCl) as the reference electrode in an electrochemical cell.

The surface morphology of the samples was analyzed using an atomic force microscope (AFM) (model NTEGRA Prima, NT-MDT, Russia) and Raman spectrometer (model Renishaw inVia, Renishaw, England).

To examine the existence of PtNPs, transmission electron microscope (TEM) images of the sample were obtained by Tecnai G2 F20 instrument (Philips Holland) equipped with an energy-dispersive X-ray spectroscopy (EDX) analyzer.

2.3. Preparation of the p-FWCNTs/AUT/Au and p-FWCNTs/Thionine/Au surfaces

Gold substrates were prepared by vacuum sputtering 150 nm Au (99.99%) on the quartz wafer. Before use, the Au substrates were cleaned in Piranha solution, a mixture of concentrated H_2SO_4 (98%) and H_2O_2 (30%) (3/1, v/v), at 90 °C for 10 min, followed by rinsing with copious water and absolute ethanol successively, dried in a stream of high-purity N_2. For fabricating the self-assembly AUT or thionine monolayers terminated by amino groups via Au–S chemical bond, gold substrates were immersed in 1 mM AUT or thionine ethanol solution for 24 h. Prior to surface condensation with carboxylic acid groups at FWCNTs ends, the monolayer coated gold substrates were washed with ethanol to rinse off residual AUT or thionine molecules and then dried in a stream of high-purity N_2. 10 mg of raw FWCNTs were chemical shortened and functionalized in 10 mL mixture of concentrated sulfuric acids (98%) and nitric acids (70%) (3/1, v/v) under ultrasonication at 40 °C for 8 h to make FWCNTs carboxyl-terminated. The reaction mixture was then diluted with doubly distilled water and centrifuged repeatedly until pH became nearly neutral. The obtained FWCNTs pipes were dried in vacuum, then spread in absolute ethanol and sonicated until 0.2 mg/mL dark-brown-colored suspension was made. Before use 0.5 mg/mL DCC was added into the suspension used as condensation agent and the mixture was ultrasonicated for 10 min, then solutions were deoxygenated by blowing high-purity N_2 for 5 min.

After that, the AUT- or thionine-modified Au substrates were immersed into FWCNTs solution for 1 h with an DC electric field to assist FWCNTs assembly, the distance between the AUT- or thionine-modified substrates and bare Au substrate which were used as anode and cathode correspondingly is 100 μm. The 10 V dc potential was applied by a regulated DC power supply. FWCNTs were aligned on the AUT and thionine self-assembly Au substrates, functionalized FWCNTs terminated by negatively charged carboxyl groups, AUT and thionine which were self-assembled on the Au substrates via Au–S bond terminated by positively charged amino groups. Under the action of the applied electric field, the negatively charged FWCNTs drift and gather onto the surface of the positively charged AUT or thionine-modified Au substrates, formed amide bond through dehydration condensation in aid of DCC, perpendicularly immobilized on Au surface.

2.4. Preparation of PtNPs modified H_2O_2 sensor and the $(PDDA/GO_x)_8/(PAA/PVS)_3$/p-FWCNTs/Thionine/Au glucose biosensor

Au electrodes were carefully polished with polishing paper (grid 3000–10,000), and subsequently with alumina until mirror finish were obtained. The as-prepared p-FWCNTs/Thionine modified Au electrode was immersed in 30 mL deposition solution (0.1 M PBS containing 10 mM K_2PtCl_6) and applied a constant potential at −200 mV for 6 min to obtain the PtNPs/p-FWCNTs/Thionine modified Au electrode.

The multilayer films $(PDDA/GO_x)_8/(PAA/PVS)_3$ on p-FWCNTs/Thionine/Au electrode were produced by the layer-by-layer self assembly technique followed the procedure described in our previous publications (Qin et al., 2009; Wu et al., 2009).

3. Results and discussion

3.1. Characterization of p-FWCNTs/AUT/Au and p-FWCNTs/Thionine/Au surfaces

Atomic force microscopic (AFM), Raman spectroscopy are powerful tools in characterizing the orientation of CNTs on solid surfaces. The typical tapping-mode AFM images of the shortened and carboxyl-terminated FWCNTs which were perpendicularly immobilized on the AUT- or thionine-modified Au surfaces by the electric field-assisting wet chemical approaches are shown in Fig. 1. The clean Au surface (Fig. 1A) before coating with FWCNTs is smooth and flat. A monolayer of densely packed, forest-like bundles can be seen on the AFM images of p-FWCNTs/AUT/Au (Fig. 1B) and p-FWCNTs/Thionine/Au (Fig. 1C) surfaces, confirming that FWCNTs is perpendicularly fixed on the AUT- or thionine-assembled Au surfaces. From the AFM images, the average lateral dimensions of nanotubes is about 70 nm, although these data do not directly reflect the true lateral sizes of nanotubes because of the broadening effect of the AFM tip (Keller, 1991). Taking into account an individual carbon tube diameter of 5 nm and the AFM tip used in our work has a typical curvature radius of ca.10 nm, we can roughly estimate the true diameter of the nanotubes aggregation is about 45 nm, indicating that FWCNTs hardly occurs aggregation during surface condensation. In addition to above mentioned, FWCNTs were also perpendicularly aligned more uniformly and closely in our work compared with perpendicularly aligned SWCNTs reported in similar studies (Wu et al., 2001), originating from the fact that FWCNTs have far less aggregates than SWCNTs. It is noted that the density of the p-FWCNTs/AUT/Au and p-FWCNTs/Thionine/Au is similar with each other, illustrating that thionine is a suitable material for vertically aligning FWCNTs on Au surface.

Raman spectroscopy (514 nm laser excitation) was used to evaluate the structure of the p-FWCNTs/Thionine/Au and p-FWCNTs/AUT/Au surfaces compared with randomly dispersed

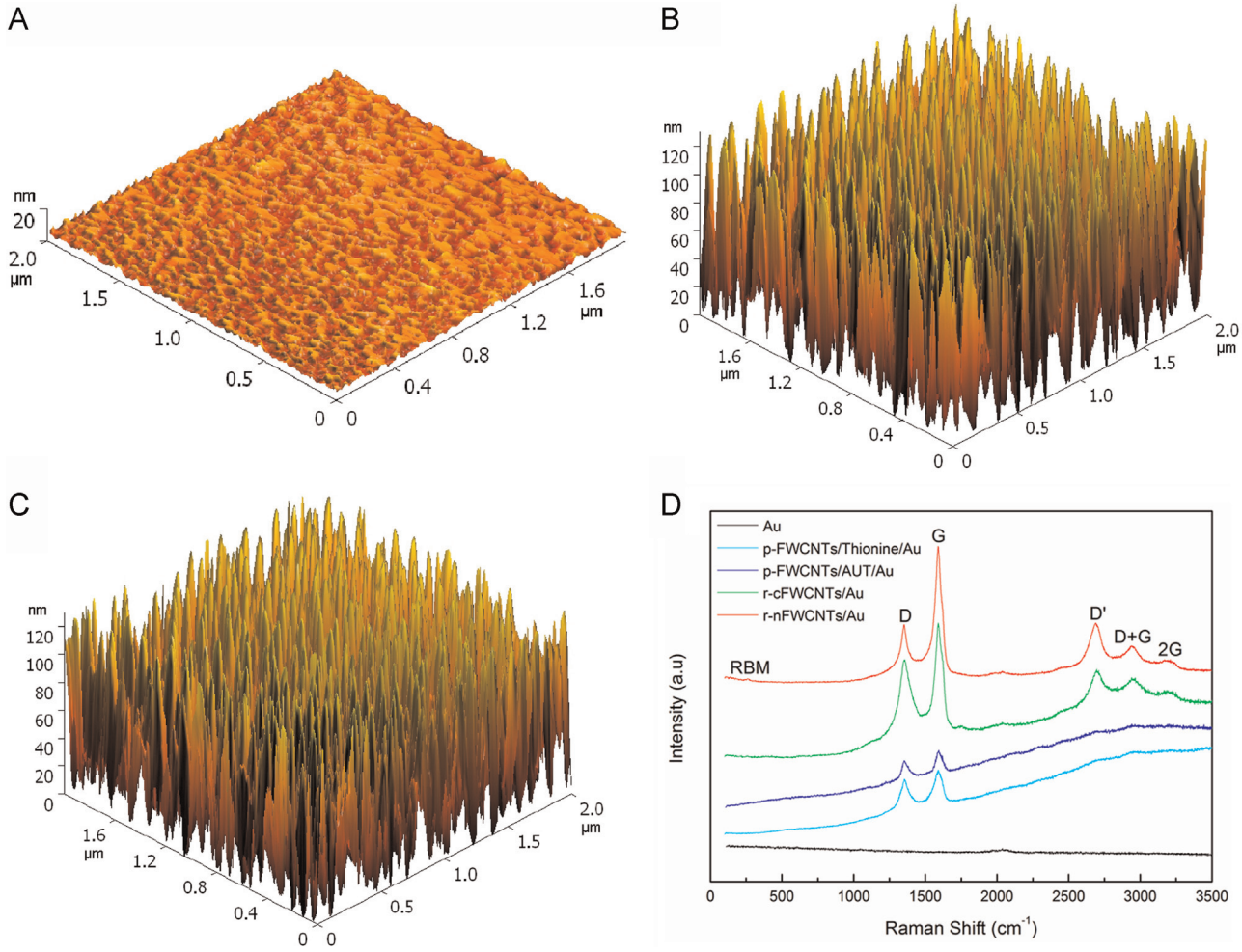

Fig. 1. Typical AFM images of FWCNTs perpendicularly immobilized on the AUT (B) and thionine assembled Au surface. (C) An image of unmodified Au surface is also reported as a control. (A) Raman spectra (D) of unmodified Au, p-FWCNTs/AUT/Au, p-FWCNTs/Thionine/Au, r-cFWCNTs/Au and r-nFWCNTs/Au surfaces excited with a laser wavelength of 514 nm.

shortened carboxyl-terminated FWCNTs (r-cFWCNTs), randomly dispersed non-carboxylated FWCNTs (r-nFWCNTs) and unmodified Au (Fig. 1D). Some distinctive peaks located between 100 and 3500 cm^{-1} of carbon nanotubes are clearly visible in the Raman spectra of the four types FWCNTs while no any peak on the surface of unmodified Au used as control. The G band centered around 1590 cm^{-1} is assigned to the in-plane C=C E_{2g} zone-center mode of graphitic structures, the D band located around 1350 cm^{-1} originates from a double resonance process induced by lattice disorder or defects in the graphite sheet (Macdonald et al., 2012). The degree of the carbon nanotubes disorder level is evaluated by the intensity ratio of the D to G peaks ($R=I_D/I_G$). The amount of defects sites caused by acid treatment would improve carbon nanotubes disorder level, are proportional to the intensity of the D peak, so the I_D/I_G values of r-nFWCNTs/Au and r-cFWCNTs/Au are 0.39 and 0.63 respectively. For vertically aligned FWCNTs, a larger portion ends of the carboxyl-terminated FWCNTs containing much defect sites (Talla et al., 2010) are exposed, while most of the exposed area is the walls in randomly dispersed carboxyl-terminated FWCNTs, so perpendicularly aligned terminus-carboxylated FWCNTs have higher I_D/I_G (Liu et al., 2009), the I_D/I_G values of p-FWCNTs/AUT/Au and p-FWCNTs/Thionine/Au are 0.82, 0.89 correspondingly. The I_D/I_G of p-FWCNTs/AUT/Au and p-FWCNT/Thionine/Au is similar to each other and much higher than that of r-cFWCNTs/Au, showing that FWCNTs were indeed perpendicularly fixed on the AUT- or thionine-modified Au surface. The intensity of D band and G band in r-cFWCNTs/Au and r-nFWCNTs/Au Raman spectra is higher than those of p-FWCNTs/AUT/Au and p-FWCNTs/Thionine/Au, because the quantities of FWCNTs on unit area of r-cFWCNTs and r-nFWCNTs which were dropped onto Au surface are larger than those of the two others, and so it is, the low coverage of the perpendicularly aligned FWCNTs lead to the increased fluorescence intensity of gold base, coupling with the fluorescence of the groups containing hydrogen introduced by acid treatment, resulted in that D· band (2700 cm^{-1}), D+G band (2940 cm^{-1}) and 2 G band (3180 cm^{-1}) in p-FWCNTs/AUT/Au and p-FWCNTs/Thionine/Au Raman spectra were annihilated and not observable, while these bands in r-cFWCNTs/Au and r-nFWCNTs/Au Raman spectra are clearly visible. The characteristic band radial breathing mode (RBM) of CNTs in the low frequency region is only fuzzy visible for the r-nFWCNTs/Au while can not be observed in others, owing to that the intensity of the RBM feature is weak and hardly observable for large diameter tubes (dt > 2 nm) and the nanotube lattice distortions caused by the acid treatment.

3.2. Electrochemical behaviors of p-FWCNTs/AUT and p-FWCNTs/Thionine modified Au electrodes

Cyclic voltammograms (CVs) of ferricyanide system showed that the electrochemical performance was improved by using thionine replace AUT to perpendicularly immobile FWCNTs on Au surface, shown in Fig. 2. The electroactive surface areas of the different electrodes were estimated by CVs in 5 mM $[Fe(CN)_6]^{3-}$ at the same scan rates according to the Randles–Sevcik Eq. (1) (Chen et al., 2012b).

$$I_p = 2.69 \neg 10^5 n^{3/2} A C_0 D_R^{1/2} v^{1/2} \quad (1)$$

where I_p refers to the peak current, n is the electron transfer number, C_0 is the concentration of the probe molecule in the solution, A represents the area of electrode, D_R is the diffusion coefficient and v is the scan rate. The electroactive surface area of AUT/Au, Thionine/Au, p-FWCNTs/AUT/Au, p-FWCNTs/Thionine/Au is about 0, 1.08, 0.95 and 1.17 times higher than the unmodified Au electrode, respectively. The results indicate that insulating AUT

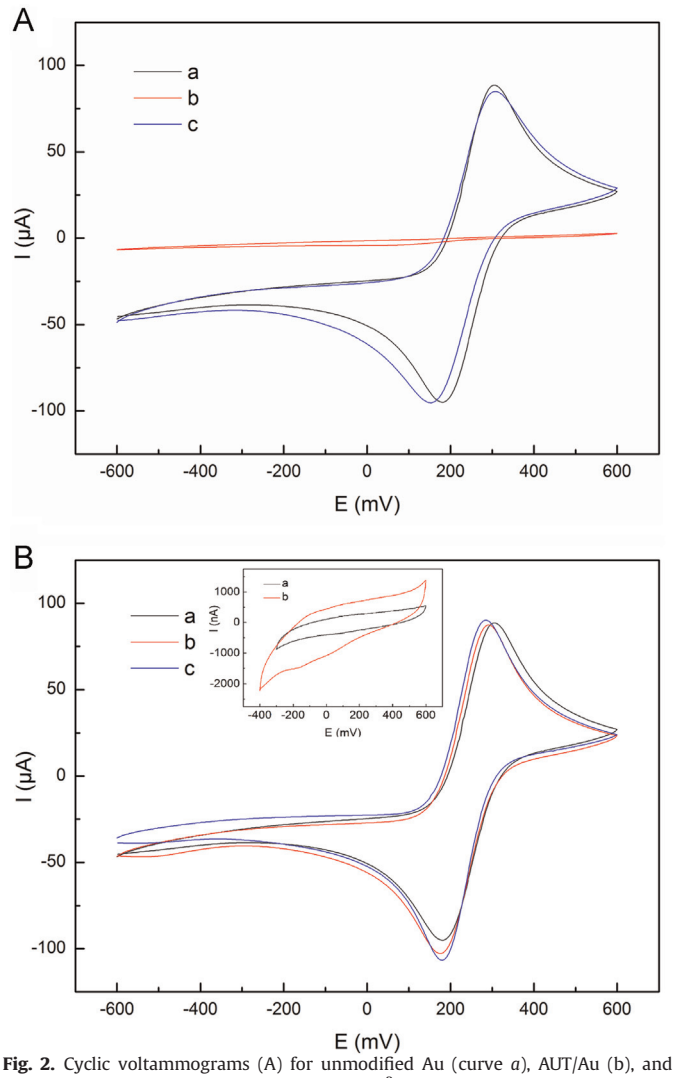

Fig. 2. Cyclic voltammograms (A) for unmodified Au (curve *a*), AUT/Au (b), and p-FWCNTs/AUT/Au (c) electrodes in $[Fe(CN)_6]^{3-}$. Cyclic voltammograms (B) for unmodified Au (a), Thionine/Au (b), and p-FWCNTs/Thionine/Au (c) electrodes in $[Fe(CN)_6]^{3-}$. Inset in B shows cyclic voltammograms for unmodified Au electrode (a) and Thionine/Au electrode (b) in PBS (scan rate of 100 mV s^{-1}).

layer completely hindered the electron transfer, while thionine can accelerate the electron exchange between Au electrode and $[Fe(CN)_6]^{3-}$ because it is an excellent electron transfer mediator. For p-FWCNTs/AUT/Au electrode, although Diao and Liu et al. claimed that the electron communication between the Au electrode and the CNTs can be realized through an electron tunneling process across the insulating AUT monolayer (Diao and Liu, 2005), but the performance of the electrode was still affected by the insulation of AUT. It is worth noting that electroactive surface area of the p-FWCNTs/Thionine/Au electrode is higher than that of p-FWCNTs/AUT/Au electrode and previously reported results for SWCNTs (Ozoemena et al., 2007). There may be four possible reasons for this improvement: Firstly, thionine could facilitate electron transfer compared with AUT. Second, larger amount of FWCNTs had been immobilized more uniformly on the Au electrode surface. Third, enhanced heat and chemical corrosion resistance make FWCNTs maintaining the structural integrity of the inner layers even if the outermost layer and extremity is functionalized in strong acid, and the better structural integrity of carbon nanotubes lead to the better conductivity. The higher conductivity and field emission performance of FWCNTs is also

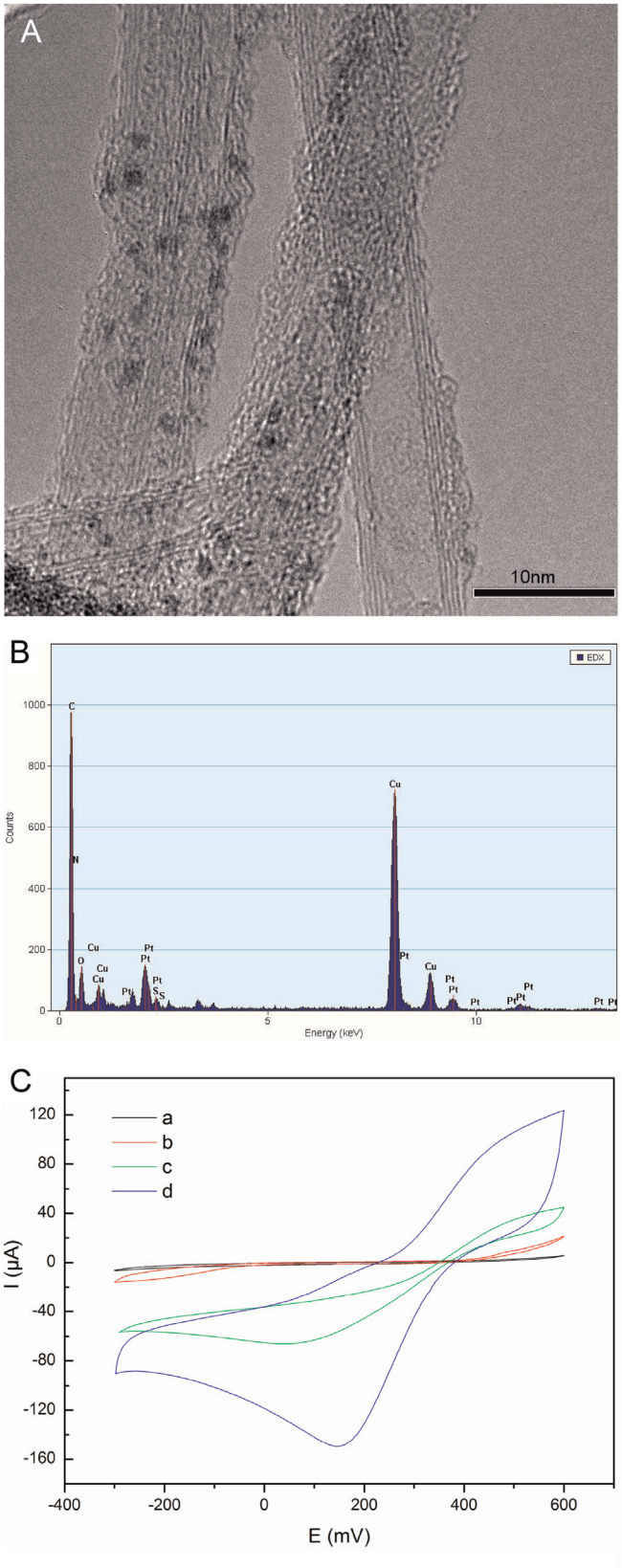

Fig. 3. TEM image (A) and EDX spectrum (B) of PtNPs/p-FWCNTs/Thionine/Au electrode. Cyclic voltammograms (C) of Thionine/Au (curve *a*), p-FWCNTs/Thionine/Au (b), PtNPs/Thionine/Au (c) and PtNPs/p-FWCNTs/Thionine/Au (d) electrodes in N_2-saturated PBS containing 2.5 mM H_2O_2 (scan rate of 100 mV s^{-1}).

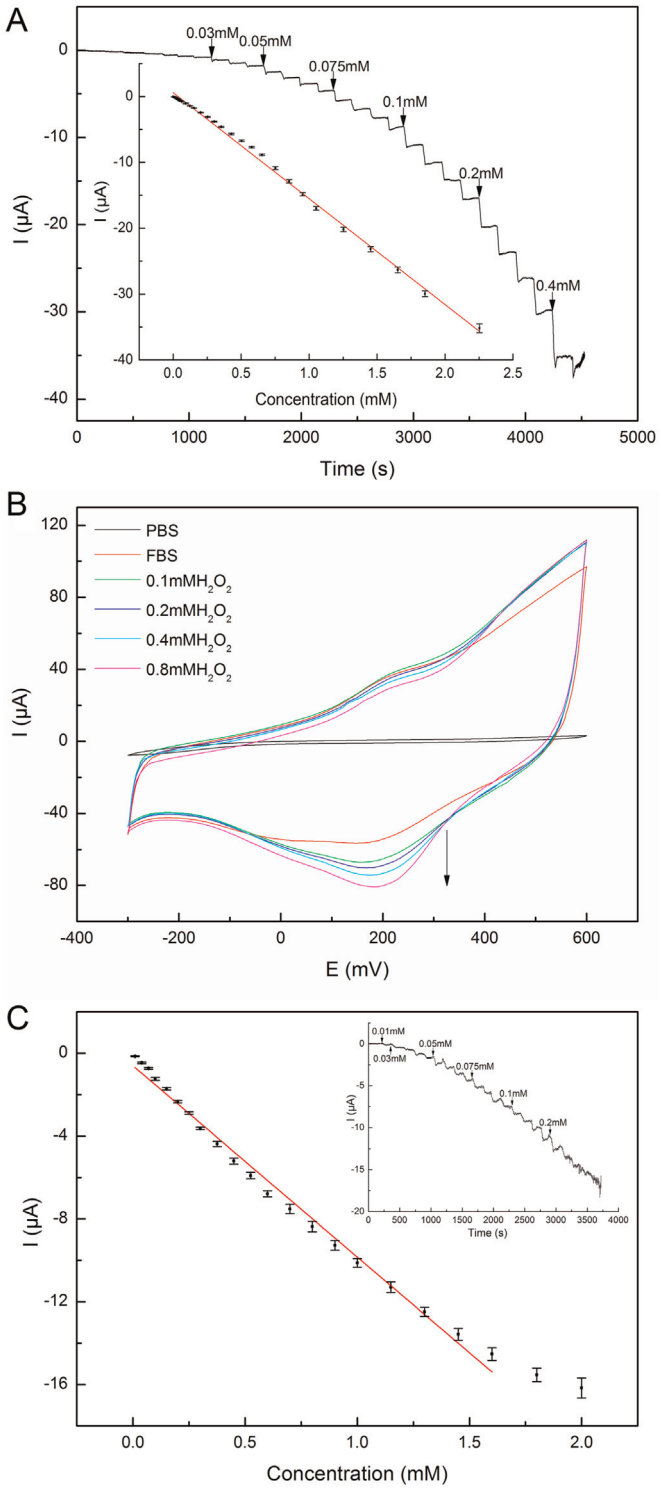

Fig. 4. Typical Chronoamperometry diagram (A) of the PtNPs/p-FWCNTs/Thionine/Au to successive addition of different concentration H_2O_2 into stirring N_2-saturated PBS at 200 mV. Inset: the calibration curve. Cyclic voltammograms (B) and calibration curve (C) of the sensor applied for detecting H_2O_2 in FBS, inset of C: the Chronoamperometry diagram of the sensor to the successive addition of different concentrations H_2O_2 into stirring N_2-saturated FBS (FBS was diluted 100 times with 0.1 M PBS at pH 7.0, applied potential: 200 mV, scan rate: 100 mV s^{-1}). Error bars indicate the standard deviations of 3 repeated measurements.

another reason for the improved performance. Moreover, the characteristic peaks of thionine at −0.4–0 V appeared on curve *b* in the inset of Fig. 2B showing that thionine was successfully self-assembled on the surface of gold electrode.

Table 1a
Comparison to performance of PtNPs or CNT non-enzymatic H_2O_2 sensor.

Sensors	Sensitivity ($\mu A\ mM^{-1}\ cm^{-2}$)	Liner range (mM)	LOD (μM)	Applied potential (V)	Ref.
Pt/Polypyrrole	80.4	1–8	1.2	−0.1	Bian et al., 2013
PtIr on Nafion solubilized MWCNTs	58.8	0.0025–0.075	2.5	+0.25	Chen et al., 2012a
Pt/TiO_2/CNT	0.85	0.004–1.25	4	+0.3	Cui et al., 2008
PVA–MWCNTs–PtNPs	122.63	0.002–8	0.7	0	Fang et al., 2012
Carbon nanotubes/iron oxide	2.74	0.099–6.54	53.6	−0.5	Miao et al., 2009
MWCNT/AgNPs	20.10	0.05–17	0.5	−0.2	Zhao et al.,. 2009
PtNPs/a-FWCNT/Thinion/Au	229.7	0.005–2.3	0.37	+0.15	This work

Table 1b
Determination of H_2O_2 in disinfected fetal bovine serum (FBS) samples using PtNPs/p-FWCNTs/Thionine/Au non-enzymatic sensor.

Sample[a]	Added (mM)	Found (mM)	RSD (%, $n=6$)	Recovery (%)
1	0.10	0.103	4.17	103
2	0.20	0.209	3.62	104.5
3	0.40	0.398	3.41	99.5
4	0.80	0.818	3.18	102.3
5	1.20	1.222	3.13	101.8
6	1.60	1.509	4.26	94.3

[a] The FBS was diluted 100 times with 0.1 M PBS (pH=7.0).

3.3. *Electrodeposition of PtNPs on p-FWCNTs/Thionine/Au for fabricating non-enzymatic H_2O_2 sensor*

In order to prove the p-FWCNTs/Thionine/Au surface is a good platform for the construction of various sensors, we fabricated a novel non-enzyme H_2O_2 sensor by electrodepositing Pt nanoparticles (PtNPs) on it. The TEM image of morphology displays that the PtNPs have decorated on the p-FWCNTs successfully by electrodeposition (Fig. 3A). The chemical composition of the surface was determined by EDX (Fig. 3B). The EDX analysis further confirmed the existence of Pt elements, O and C peaks originated from the p-FWCNTs, S and N peaks arising from thionine, and Cu peak due to the substrate. These results illustrate that the PtNPs have been deposited onto p-FWCNTs/Thionine/Au.

Voltammetric methods were used to study the catalytic activities of the as-prepared PtNPs/p-FWCNTs/Thionine/Au non-enzyme sensors to H_2O_2, shown in Fig. 3C. A pair of weak redox peaks emerged on p-FWCNTs/Thionine/Au electrode, while no redox peak was found on the Thionine/Au electrode. This is probably because the perpendicularly aligned FWCNTs greatly increased the specific surface area of the electrode. The current of redox peaks on PtNPs/Thionine/Au electrodeobviously increased, indicating the response to H_2O_2 of the sensor is enhanced by the modification of PtNPs, but the response signal was significantly lower than PtNPs/p-FWCNTs/Thionine/Au electrode. This demonstrated perpendicularly immobilized FWCNTs greatly increased specific surface area and enlarged the amount of PtNPs, resulting in the enhanced catalytic activity to H_2O_2.

3.4. *Variables optimization and performance of non-enzymatic H_2O_2 sensors*

The experimental variables including electrodeposited time and the concentration of K_2PtCl_6 have been optimized through steady-state response current and chronoamperometry on the successive addition of H_2O_2, shown in Fig. S1. According to the changes of response current, sensitivity and the signal/noise ratio, we selected deposition time of 6 min and the K_2PtCl_6 concentration of 10 mM as the optimized conditions in this work.

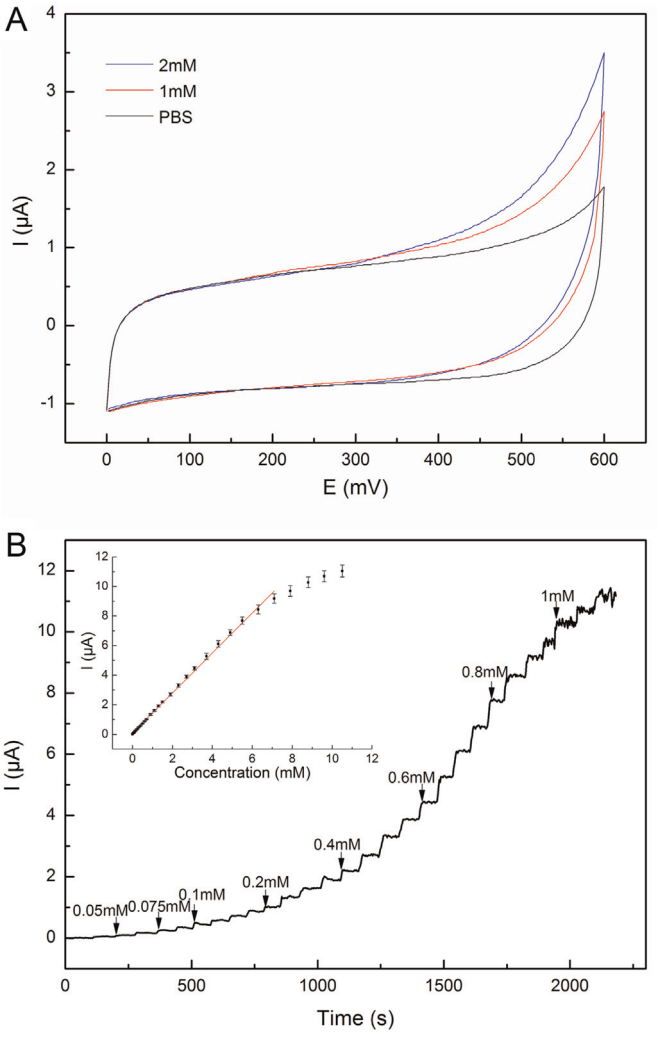

Fig. 5. Cyclic voltammograms (A) of $(PDDA/GO_x)_8/(PAA/PVS)_3$/p-FWCNTs/Thionine/Au (scan rate of 100 mV s^{-1}). Chronoamperometry diagram (B) of glucose biosensor to the successive addition of different concentration glucose into stirring PBS at 600 mV. Inset: the calibration curve. Error bars indicate the standard deviations of 3 repeated measurements.

The relative standard deviation (RSD) of current signal to 1 mM H_2O_2 of the obtained PtNPs/p-FWCNTs/Thionine/Au was less than 4.32% for six modified Au electrodes prepared at the same conditions. The current response for 1 mM H_2O_2 sensor retained more than 98% of its original response after 7 days and 91.3% after 30 days, during storage at 4 °C. The good reproducibility and stability is largely attributed to that the p-FWCNTs were firmly immobilized on the thionine self-assembled gold electrode through amide bonds.

Table 1c
Determination and recovery studies of glucose in human serum samples using $(PDDA/GO_x)_8/(PAA/PVS)_3$/p-FWCNTs/Thionine/Au glucose biosensor.

Sample no.	Hospital method founded[a] (mM)	Determined by biosensor (mM)	RSD (%, $n=6$)	Glucose added (mM)	Glucose found (mM)	Recovery (%)	RSD (%, $n=6$)
1	2.30	2.19	3.82	1.00	0.93	93	3.39
2	2.45	2.54	2.98	1.00	1.05	105	3.16
3	2.65	2.73	3.05	1.00	0.92	92	2.87
4	2.75	2.87	3.52	2.00	1.87	90.5	4.18
5	2.90	2.79	3.74	2.00	1.91	92.5	3.83
6	3.05	2.92	4.21	2.00	2.16	108	3.91

[a] The glucose concentrations of each serum samples were diluted one multiple with 0.1 M PBS (pH=7.0).

To evaluate the selectivity of the proposed sensor, the effects of several possible electroactive interferents such as urea acid (UA), dopamine (DA) and ascorbic acid (AA) were examined (Fig. S2). There was no response to successive addition of the possible interfering compounds, showing that the PtNPs/p-FWCNTs/thionine/Au sensor was highly selective to H_2O_2.

3.5. Determination of H_2O_2 by PtNPs/p-FWCNTs/Thionine/Au non-enzymatic sensor

We expect that perpendicularly aligned FWCNTs through thionine can provide greater specific surface area and facilitate electron transfer to PtNPs for improving the performance of as-prepared H_2O_2 sensors. Chronoamperometry diagram of PtNPs/p-FWCNTs/Thionine/Au non-enzyme H_2O_2 sensor is presented in Fig. 4A. Inset shows the calibration curve of the sensor, which exhibits a wide linear range for H_2O_2 from 5 μM to 2.3 mM with a correlation coefficient 0.997, a amazing sensitivity of 229.7 μA mM^{-1} cm^{-2}, and low detection limit (LOD) is 0.37 μM at the signal/noise ratio of 3 (S/N=3). The response time to reach 95% of the maximum steady-current is within 5 s. To evaluate the performance of as-prepared H_2O_2 sensor, a comparison of applied potential, sensitivity, LOD and linear range for this work with other PtNPs or CNTs non-enzymatic H_2O_2 sensors was shown in Table 1a. Our results in LOD and linear range are comparative to other sensors and the sensitivity is obviously higher than others, showing that p-FWCNTs/Thionine/Au electrodes could be used as an excellent platform for fabricating sensors.

The capability of the proposed sensor for practical applications was investigated to detected H_2O_2 in disinfected fetal bovine serum (FBS). Firstly, cyclic voltammograms (CVs) of PtNPs/p-FWCNTs/Thionine/Au sensor at −0.3–0.6 V in the FBS sample and PBS used as control are measured and compared to obtain the current baseline of serum background, shown in Fig. 4B. The CVs in Fig. 4B clearly depict that current of the peaks at 200 mV increased significantly as the H_2O_2 concentrations increased, confirming that the peak corresponds to the reduction of H_2O_2. So we chose 200 mV as the applied voltage to assess the ability of the sensor for detection H_2O_2 in practical samples through chronoamperometry measurement (in inset of Fig. 4C). The calibration curve of PtNPs/p-FWCNTs/Thionine/Au electrode for H_2O_2 detection in FBS (Fig. 4C) shows that when the sensor was used in diluted FBS solution, it still has a fine linear current response to H_2O_2 ranging from 10 μM to 1.6 mM ($R^2=0.991$). The sensitivity of the sensor to H_2O_2 in FBS is up to 132.1 μA mM^{-1} cm^{-2}, the detection limit is 1.14 μM (S/N=3). The results indicate that the sensor has great potential in testing H_2O_2 in real samples. The recovery tests for H_2O_2 were performed through the standard addition method which is adding H_2O_2 of different known concentrations into the FBS samples. The concentration of H_2O_2 in serum samples was determined to be 1.7 ± 0.2 μM ($n=3$) by chronamperometry measurement. The calculated recovery values were in the range of 94.3–104.5% and shown in Table 1b, indicating that the sensor can be successfully applied for the detection of H_2O_2 in real samples.

3.6. Performance of the $(PDDA/GO_x)_8/(PAA/PVS)_3$/p-FWCNTs/Thionine/Au glucose biosensor

We also prepared a glucose biosensor to verify p-FWCNTs/Thionine/Au could be used for the fabrication of enzyme-based biosensor. Fig. 5A shows the cyclic voltammograms of $(PDDA/GO_x)_8/(PAA/PVS)_3$/p-FWCNTs/Thionine/Au electrode measured without and with the addition of different concentration glucose in PBS. The oxidation current around 600 mV increased significantly with the increase of glucose concentration, indicating the response of the enzyme electrode to glucose. The typical amperometric response of the $(PDDA/GO_x)_8/(PAA/PVS)_3$/p-FWCNTs/Thionine/Au glucose biosensor was shown in Fig. 5B, conducted on successive injection of different concentration glucose into the stirring PBS at an applied potential of 600 mV. The calibration curve (inset in Fig. 5B) is linear over a glucose concentration from 0.05 to 6.3 mM ($R^2=0.997$) and a high sensitivity of 19.01 μA mM^{-1} cm^{-2} (1.35 μA/mM). The detection limit is estimated to be about 11 μM (S/N=3). The sensitivity of the as-prepared glucose biosensor is better than those glucose biosensor we had constructed through the similar methods previous reported 0.45 μA/mM (Wu et al., 2009), 0.555 μA/mM (Wu et al., 2007). It could be attributed to the large surface-to-volume ratio, high conductivity and facilitate electron transfer of the p-FWCNTs/Thionine/Au basement, indicating it is a good platform for construction of enzyme-based biosensor.

The response current of this glucose biosensor retained 90.7% of its initial response current after being stored at 4 °C for 15 days. The relative standard deviation (RSD) of the current response to 0.5 mM glucose is 3.4% for 5 successive measurements. Several typical interferences including ascorbic acid (AA), acetaminophen (AP) and uric acid (UA) are chosen to test the selectivity of the biosensor for glucose detection, in which no apparent interferences are observed (Fig. S3).

In order to illustrate the practical usage of this biosensor, it was applied to detect the glucose in six different human serum samples from a local hospital. The results (Table 1c) obtained from the glucose sensor are consistent with that of hospital method. The recovery were investigated by standard additions of glucose and in the range of 90.5–108%, RSD ranged from 2.87% to 4.21%, indicating that the glucose sensor could be used for glucose detection in human serum.

4. Conclusions

In this work, we have perpendicularly immobilized FWCNTs on thionine assembled Au surface through the wet chemical method for the first time. It proved that thionine can be used to take place of AUT to realize highly ordered alignment of FWCNTs. The p-FWCNTs/Thionine/Au surface we have constructed was uniform and with high surface area, which suppressed aggregation of FWCNTs. Furthermore, the as-prepared electrode showed better current response and facilitated electron transfer. The covalently bounded FWCNTs avoid the fall off phenomena of the CNTs immobilized by drop coating method. On the basis of these three points, we developed hydrogen peroxide sensor by electrodeposition of PtNPs and glucose biosensor through layer-by-layer self assembly of $(PDDA/GO_x)_8/(PAA/PVS)_3$ film, the resultant sensors own better sensitivity, good linear range and low detection limit, proved p-FWCNTs/Thionine/Au surface we had innovatively developed own excellent electrochemical properties, coupled with abundant carboxyl groups at the end of p-FWCNTs can provide an ideal platform for fabricating diverse sensors.

Acknowledgements

This work was financially supported by the National Natural Science Foundation of China. (Grant nos. 81127001 and 81273993).

Appendix A. Supplementary Information

Supplementary data associated with this article can be found in the online version at http://dx.doi.org/10.1016/j.bios.2014.09.057.

References

Baughman, R.H., Zakhidov, A.A., Heer, W.A., 2002. Science 297, 787–792.
Bian, X., Lu, X., Jin, E., Kong, L., Zhang, W., Wang, C., 2013. Talanta 81, 813–818.
Chen, K.J., Chandrasekara Pillai, K., Rick, J., Pan, C.J., Wang, S.H., Liu, C.C., Hwang, B.J., 2012a. Biosens. Bioelectron. 33, 120–127.
Chen, Q., Zhou, J., Han, Q., Wang, Y.H., Fu, Y.Z., 2012b. Colloids Surf. B 92, 130–135.
Chen, X., Cai, Z., Huang, Z., Oyama, M., Jiang, Y., Chen, X., 2013. Electrochim. Acta 97, 398–403.
Chou, A., Bçcking, T., Singh, N.K., Gooding, J.J., 2005. Chem. Commun., 842–844.
Cui, X., Li, Z., Yang, Y., Zhang, W., Wang, Q., 2008. Electroanalysis 20, 970–975.
Diao, P., Liu, Z., 2005. J. Phys. Chem. B 109, 20906–20913.
Diao, P., Liu, Z., 2010. Adv. Mater. 22, 1430–1449.
Fang, Y., Zang, D., Qin, X., Miao, Z., Takahashi, S., Anzai, J., Chen, Q., 2012. Electrochim. Acta 70, 266–271.
Gooding, J.J., Wibowo, R., Liu, J., Yang, W., Losic, D., Orbons, S., Mearns, F.J., Shapter, J.G., Hibbert, D.B., 2003. J. Am. Chem. Soc. 125, 9006–9007.
Heer, W.A., Chatelain, A., Ugarte, D., 1995. Science 270, 1179–1180.
Huang, L., Jia, Z., Brien, S.O.′, 2007. J. Mater. Chem. 17, 3863–3874.
Janyasupab, M., Liu, C.W., Zhang, Y., Wang, K.W., Liu, C.C., 2013. Sens. Actuators, B 179, 209–214.
Keller, D., 1991. Surf. Sci. 253, 353–364.
Liu, X., Baronian, K.H.R., Downard, A.J., 2009. Carbon 40, 500–506.
Liu, Y., Liu, L., Dong, S., 2007. Electroanalysis 19, 55–59.
Macdonald, T., Gibson, C.T., Constantopoulos, K., Shapter, J.G., Ellis, A.V., 2012. Appl. Surf. Sci. 258, 2836–2843.
Mattos, I.L., Gorton, L., Ruzgas, T., 2003. Biosens. Bioelectron. 18, 193–200.
McEuen, P.L., Fuhrer, M.S., Park, H., 2002. IEEE Trans. Nanotechnol. 1, 78–85.
Miao, Y., Wang, H., Shao, Y., Tang, Z., Wang, J., Lin, Y., 2009. Sens. Actuators B 138, 182–188.
Nayak, S., Bhattacharjee, S., Singh, B.P., 2012. Carbon 50, 4269–4276.
Ouyang, M., Huang, J.L., Lieber, C.M., 2002. Acc. Chem. Res. 35, 1018–1025.
Ozoemena, K.I., Nyokong, T., Nkosi, D., Chambrier, I., Cook, M.J., 2007. Electrochim. Acta 52, 4132–4143.
Patolsky, F., Weizmann, Y., Willner, I., 2004. Angew. Chem. Int. Ed. 43, 2113–2117.
Peng, H.L., Chen, Z., Tong, L.M., Yu, X.C., Ran, C.B., Liu, Z.F., 2005. J. Phys. Chem. B 109, 3526–3530.
Qi, H., Qian, C., Liu, J., 2006. Chem. Mater. 18, 5691–5695.
Qian, C., Qi, H., Gao, B., Cheng, Y., Qiu, Q., Qin, L.C., Zhou, O., Liu, J., 2006. J. Nanosci. Nanotechnol. 6, 1346–1349.
Qian, C., Qi, H., Liu, J., 2007. J. Phys. Chem. C 111, 131–133.
Qin, X., Wang, H.C., Wang, X.S., Li, S., Miao, Z.Y., Huang, N., Chen, Q., 2009. Mater. Sci. Eng. C 29, 1453–1457.
Sheeney-Haj-Ichia, L., Basner, B., Willner, I., 2005. Angew. Chem. Int. Ed. 44, 78–83.
Talla, J., Zhang, D.H., Kandadai, M., Avadhanula, A., Curran, S., 2010. Phys. Rev. B: Condens. Matter 405, 4570–4573.
Wu, B., Zhang, J., Wei, Z., Cai, S., Liu, Z., 2001. J. Phys. Chem. B 105, 5075–5078.
Wu, B.Y., Hou, S.H., Yin, F., Li, J., Zhao, Z.X., Huang, J.D., Chen, Q., 2007. Biosens. Bioelectron. 22, 838–844.
Wu, B.Y., Hou, S.H., Yu, M., Qin, X., Li, S., Chen, Q., 2009. Mater. Sci. Eng. C 29, 346–349.
Yan, Y., Chan-Park, M.B., Zhang, Q., 2007. Small 3, 24–42.
Yang, J., Zhang, R., Xu, Y., He, P., Fang, Y., 2008. Electrochem. Commun. 10, 1889–1892.
Zhao, W., Wang, H., Qin, X., Wang, X., Zhao, Z., Miao, Z., Chen, L., Shan, M., Fang, Y., Chen, Q., 2009. Talanta 80, 1029–1033.